Journal of Physics: Conference Series

OPEN ACCESS

Experimental investigations in an air-filled differentially-heated cavity at large Rayleigh Numbers

To cite this article: P Belleoud *et al* 2012 *J. Phys.: Conf. Ser.* **395** 012119

View the article online for updates and enhancements.

You may also like

- Rayleigh-number evolution of large-scale coherent motion in turbulent convection
J. J. Niemela and K. R. Sreenivasan
- Convective heat transport in slender cells is close to that in wider cells at high Rayleigh and Prandtl numbers
Ambrish Pandey and Katepalli R. Sreenivasan
- On the triggering of the Ultimate Regime of convection
P-E Roche, F Gauthier, R Kaiser et al.

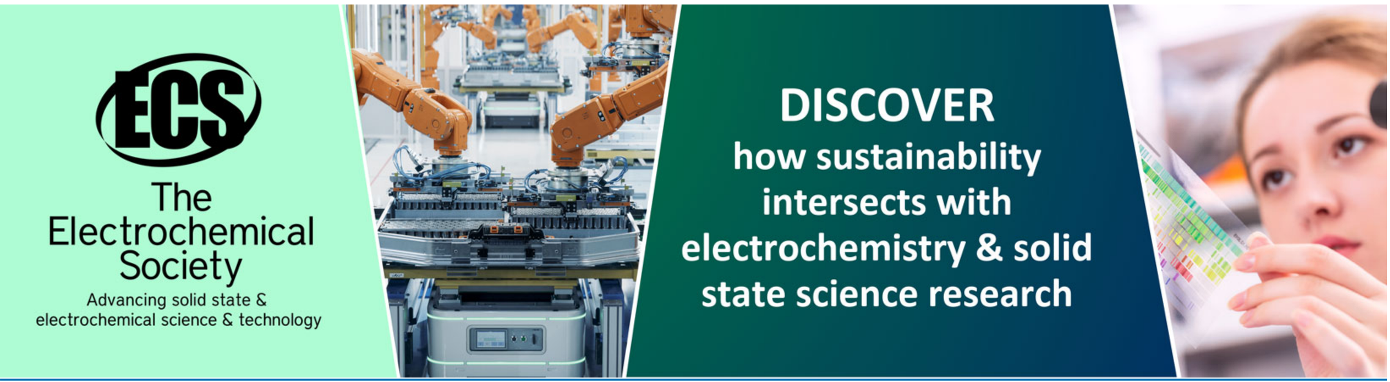

This content was downloaded from IP address 18.119.192.55 on 13/05/2024 at 17:45

Experimental investigations in an air-filled differentially-heated cavity at large Rayleigh Numbers

P. Belleoud[1,*], D. Saury[1], P. Joubert[2], D. Lemonnier[1], F. Djanna[1],

[1] Institut Pprime - UPR 3346, CNRS - ENSMA - Université de Poitiers, Fluid, Thermal and Combustion Science department, ENSMA, Téléport 2, 1 avenue Clément Ader - BP 40109, F-86961 Futuroscope cedex, France.
[2] LaSIE, FRE-CNRS 3474, Avenue Michel Crépeau, 17042 La Rochelle cedex 1, France.

[*]Corresponding author: pierre.belleoud@ensma.fr

Abstract. A large-scale experimental differentially heated cavity was built and instrumented. Rayleigh numbers up to 1.2×10^{11} can be obtained with a temperature difference, ΔT=20°C, between the hot and cold walls leaning in the range of validity of the Boussinesq approximation. Previous data obtained locally for mean velocity by 2D LDV in the range give rise to questions regarding the general air flow circulation in the cavity. Particularly, a downstream flow along the vertical boundary layer was observed. This reverse flow caused by the temperature stratification outside this layer is not present in the upstream parts and was not previously observed in smaller cavities. The question of the global circulation in this cavity is thus posed. Evolution laws providing Nusselt numbers are also given and when possible compared to the literature for a large range of Rayleigh numbers.

1. Introduction

Natural convection phenomenon is the matter of many studies especially with differentially-heated cavities [1-7] and its applications are numerous, in particular in the building sector. Indeed, the energy consumption of this field represents 45% of the global French national energy consumption. And because natural convection is involved as soon as density gradients are present, it seems necessary to try to understand this phenomenon in order to control the resulting heat exchanges. That is the purpose of these studies and the differentially-heated cavity is an interesting device to consider natural convection [3]. Several investigations have been conducted on this phenomenon at low Rayleigh numbers [1]. However, many applications (aeronautics, buildings…) need an explanation of the phenomenon at higher Rayleigh numbers ($\sim10^{11}$), for which the natural convection flow is turbulent. The purpose of this study is to provide a set of results concerning the thermal boundary layer in a cavity with a high Rayleigh number, including: temperature profiles (mean and fluctuating), some characteristics (thickness…) and correlations of the Nusselt number.

2. Experimental device

The present experiments were conducted in a 4m-high cavity filled with air having two opposite vertical “active walls”. One of these walls is cooled and the other one is heated. Both are made of aluminum plate (AU4G, thermal conductivity: $k=134\ \mathrm{W\ m^{-1}\ K^{-1}}$ and measured hemispheric global emissivity: ε=0.15) and maintained constant temperature thanks to 2 cryothermostats and a glycol-water flow. The other walls are made of 8 cm-thick polyurethane foam panels (k=0.035 W m^{-1} K^{-1}) and the outer part of the cavity is bordered by additional 3cm-thick insulation panels. Moreover, to reduce surface radiation into the cavity, the inner side of the walls is covered by a 40μm-thick low-emissivity film (ε=0.1). **Figure 1** shows a schematic view of the inside of the cavity including real dimensions and the upper part of the experimental device equipped with a 2D LDV system. Temperature is measured by K type thermocouples with a diameter of 12.7μm. The thermocouples are moved inside the cavity thanks to a 3 meters-stick mobile along the Y and Z-axes.

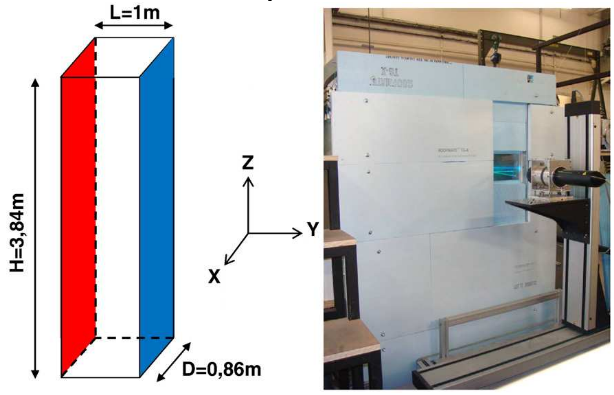

Figure 1. Scheme of inner cavity and photography of the upper part of the cavity.

3. Global flow circulation

Figure 2 shows the global flow circulation within the upper part of the cavity by presenting velocity fields and streamlines obtained in this study using Particule Image Velocimetry (PIV). These results reinforce previous assumptions [8] on the flow circulation. The main circulation follows the edges of the cavity, a recirculation zone is formed at the top of the cavity and at the border of the hot thermal boundary layer (2/3 of the cavity) and downward flow feeds the cold boundary layer. Some numerical studies have been carried out [2] and require experimental results for comparisons.

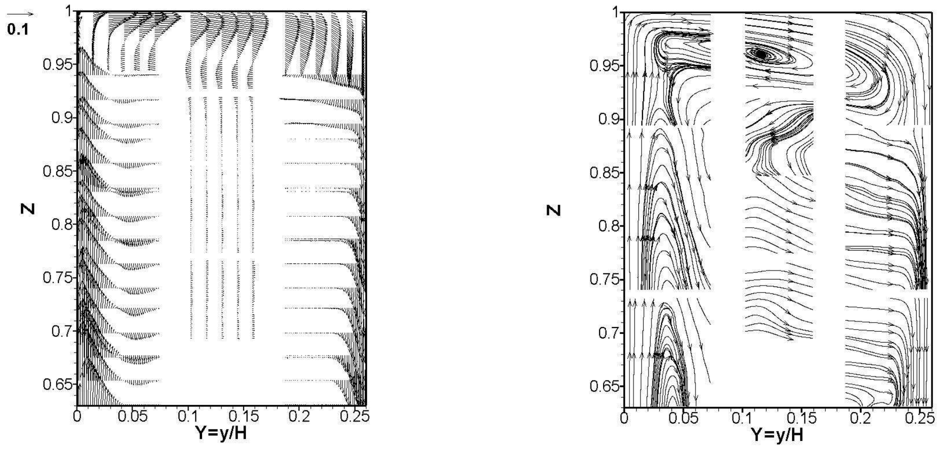

Figure 2. (a) Dimensionless mean velocity fields and (b) streamlines in the upper part of the cavity for a global Rayleigh number equal to 1.2×10^{11}.

4. Temperature fields

4.1. Centrosymmetry property

Temperature is measured at different heights along the upwards and downwards boundary layers, and in particular at two complementary locations (Z=z/H=0.70 and 0.30=1-Z), shown in **Figure 3**, underlining that, due to perfect symmetry of the problem, the temperature repartition is centrosymmetric. Indeed, the temperature profiles show that the temperature of the ascending thermal boundary layer (Z=0.70) has the same behaviour than the descending one (Z=0.30) when considering centrosymmetry: the two opposite temperature profiles at the dimensionless height of Z=0.30 and Z=0.70 are symmetrical with respect to the cavity centre. As a result, the study of the flow can be conducted on only half of the cavity. The same trend is also observed on RMS values of the temperature. Dimensionless temperature is defined by $\theta = \frac{T-T_0}{\Delta T_{ref}}$, with T, the temperature, measured with an error of 0.07°C, $T_0 = \frac{T_h+T_c}{2}$ and $\Delta T_{ref} = T_h - T_c$ knowing that T_h (30°C in this study) is the temperature of the hot wall and T_c (10°C in this study) the temperature of the cool one.

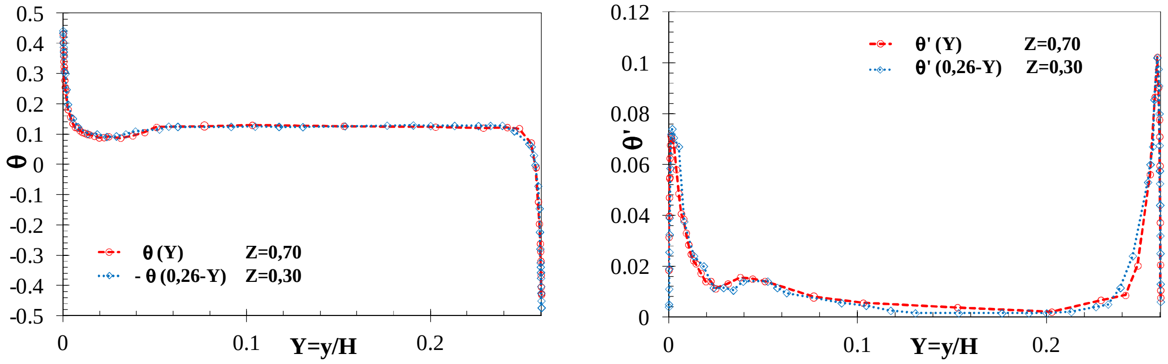

(a) (b)

Figure 3. (a) Mean of the dimensionless temperature, θ, (b) RMS fluctuation of the temperature, θ'.

4.2. Temperature field

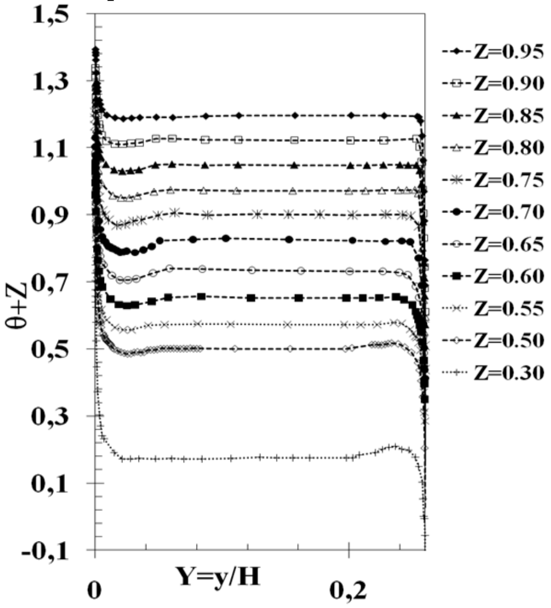

Figure 4. Dimensionless temperature, θ, profiles in the cavity at different heights for a Rayleigh number $Ra_H = 1.2\times10^{11}$.

The temperature profiles, presented in **Figure 4**, give another illustration of the centrosymmetry of the temperature repartition but also highlight the thermal stratification of the (stagnant) core for Z in [0.30, 0.95]. The detailed stratification along the centerline can be found in [8]. We notice here different behaviours in the hot thermal boundary layer:

- for Z= 0.30, the temperature across the boundary layer presents a monotonic decrease,
- for 0.50<Z<0.95, temperature decreases first to a minimum value and then, increases up to the core temperature. This trend results from a slight return flow of cool air driven upwards by the hot boundary layer from the layers, which is a typical behaviour of natural boundary layers flow in thermally stratified environment.

4.3. Thermal boundary layer

The usual definition of a thermal boundary layer thickness at a given elevation is the distance from the wall where the flow reaches a specific percentage of the core temperature at this elevation. **Figure 5** presents a graphical representation of this boundary layer thickness, δ_t, in the two cases encountered along the buoyant boundary layers, that is with or without temperature depletion zone. **Figure 6** presents the results obtained by applying these rules. It appears that the hot boundary layer gets thicker when moving upward until Z=0.40 where the local Rayleigh number, Ra_Z (eq.(1)), is about 7.36×10^9. Then, it is abruptly divided by two in the upper part of the cavity when the local Rayleigh number reaches 4.85×10^{10} (Z≈0.75) and then remains further unchanged up to Z=0.95, that is $Ra_Z=9.86\times10^{10}$. This thickness reduction could be explained by the development of vortex structures at the outer edge of the hot boundary layer. These vortices grow with the height and stop the development of the boundary layer. As expected for a centrosymmetric flow, the opposite-side cold boundary layer exhibits the same evolution in the opposite direction (i.e. 1-Z). The local Rayleigh number is defined with the following expression:

$$Ra_z = \frac{g\beta\Delta T_{ref} z^3}{\upsilon\alpha} \qquad (1)$$

With g the acceleration due to gravity, $\beta = \frac{1}{T_0}$, υ the air kinematic viscosity at T_0 and α the thermal diffusivity of the air at T_0.

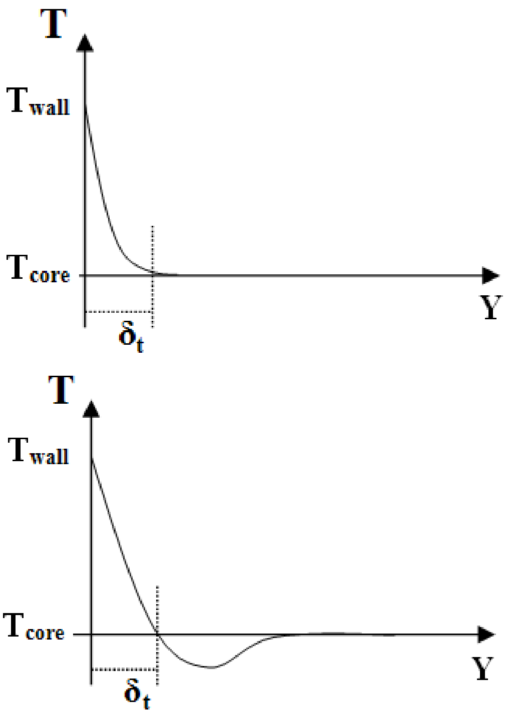

Figure 5. Definition of the thickness of the thermal boundary layer.

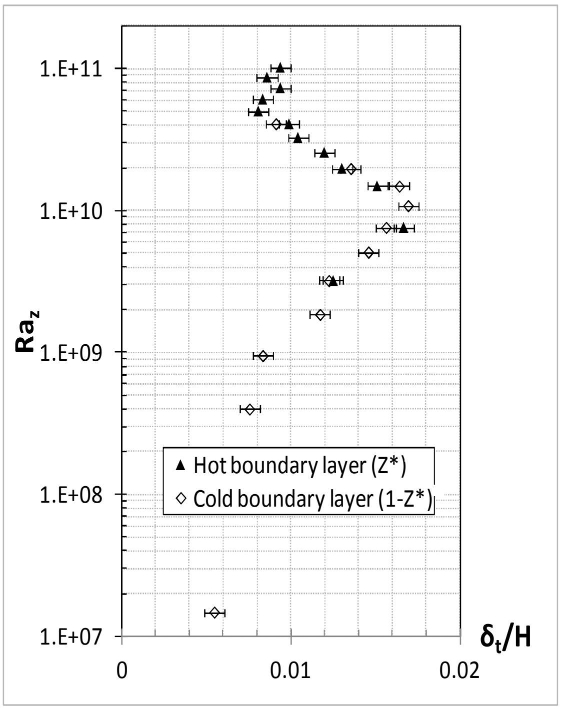

Figure 6. Evolution of the thermal boundary layers thicknesses versus the local Rayleigh number.

4.4. Temperature RMS fluctuations.

The temperature RMS fluctuations profiles across hot and cold boundary layers underline once more the centrosymmetry property of the flow. The fluctuations, shown in **Figure 7**, increase from the wall to reach a maximum at about Y=0.0018 (about 7 mm from the wall) and then decrease to become almost null outside the boundary layer.

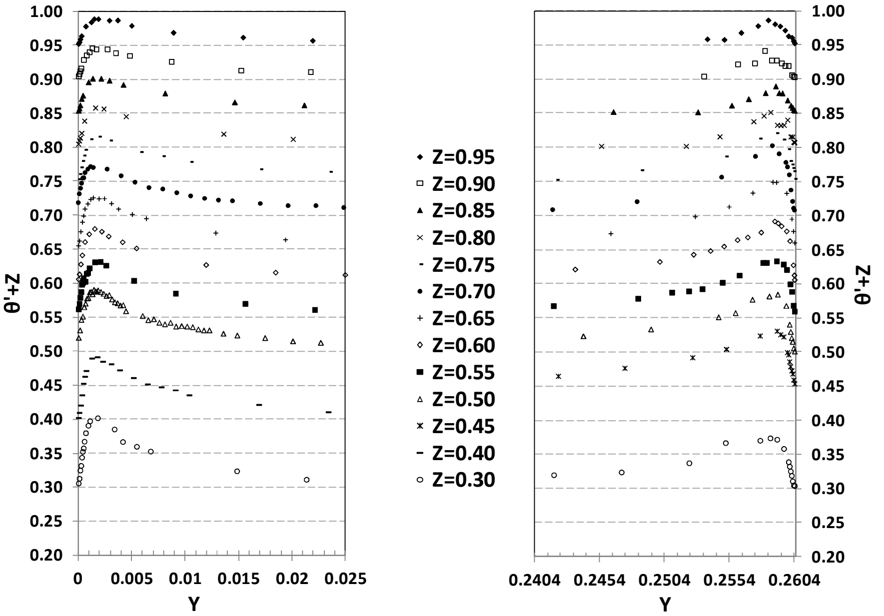

Figure 7. Profiles of the RMS fluctuation of the temperature, θ', for Ra_H 1.2×10^{11}.

4.5. High order temperature moments (kurtosis and skewness)

The 3rd and 4th order moments of temperature (or velocity) fluctuations are usually used to statistically characterise turbulent flows. Turbulence is defined "homogeneous" if these probability density functions follow a Gaussian distribution [4]. The third central moment or skewness, θ_{skew}, and the fourth central moment or kurtosis, θ_{kurt}, tell us whether the distribution is Gaussian or not (θ_{skew}=0 and θ_{kurt}=3 for a Gaussian distribution).

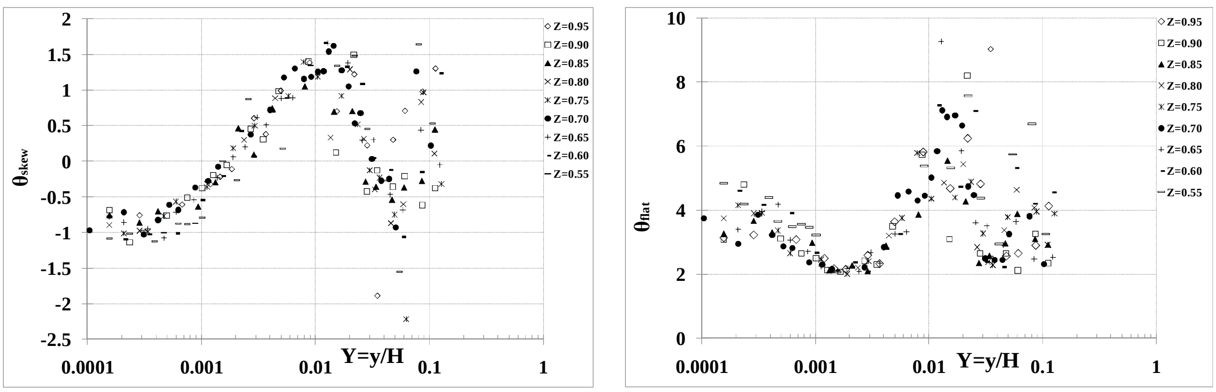

(a) (b)

Figure 8. (a) Skewness and (b) kurtosis factor of the temperature fluctuations in the hot boundary layer at different dimensionless elevations for Ra_H=1.2×10^{11}.

4.5.1. *Temperature skewness.* **Figure 8-(a)** shows different profiles of the 3rd order moment of the temperature fluctuation (skewness factor). This factor is understandably negative near the hot wall, because of the prescribed temperature condition. Then skewness values increase to reach a positive maximum at about Y=0.015 (≈5-6 cm from the wall) whatever the elevation. This location corresponds to the edge of the thermal boundary layer. The skewness value is zero for two positions: Y=0.002 (about 7 mm from the wall) where the maximum of temperature fluctuation is achieved and Y=0.035 (at about 14 cm from wall), corresponding to the shear flow area.

4.5.2. *Temperature kurtosis.* Kurtosis factor (or the 4^{th} order moment) is presented in **Figure 8-(b)**. The kurtosis factor decreases from the wall to reach a minimum value of about 2 near Y=0.002 (7 mm from the wall) and increases to a maximum at Y=0.015 (i.e. 5 cm from the wall).

We notice some similarities between skewness and kurtosis profiles. First, both have a maximum at Y=0.015 (about 5cm from the wall) and then the minimum values of kurtosis correspond to zero skewness values at Y=0.035. These two locations are related, respectively, to the (i) maximum of the vertical velocity, W and to (ii) the separation between the recirculating air flow at the outer edge of the boundary layer and the global airflow circulating around the whole cavity. These considerations could lead to another definition of the boundary layer, this time statistically speaking. These results could also eventually conduct to a rebuilding of the time signal and a discussion of the position of a shear zone (where skewness and kurtosis are maximum) between the global circulation flow and local recirculation flows.

5. Heat transfers along temperature-controlled walls

5.1. Determination of the Nusselt number

Nusselt number is used to quantify heat transfer along the walls. This parameter has been obtained by two different ways. The first consists in temperature measurements in the conductive thermal boundary layer to get the slope at the wall, $\left(\frac{dT}{dy}\right)_w$ and then the mean local Nusselt number as: Nu_z,

$$\langle Nu_z \rangle = \frac{H}{\Delta T}\left(\frac{dT}{dy}\right)_w \tag{2}$$

where, H is the height of the cavity and ΔT is the temperature difference between the active walls. A second method consists in measuring instantaneous differences of temperature with a double counter-connected microthermocouple (12.7µm in diameter) with probes distance e=500±10µm, in order to obtain the instantaneous local value of the Nusselt number, $Nu_z(t)$:

$$Nu_z(t) = \frac{H}{\Delta T}\frac{\Delta T(z,t)}{e} \tag{3}$$

Knowing the acquisition time, the mean local Nusselt number is then easily calculated by:

$$\langle Nu_z \rangle = \frac{1}{t_{aq}}\int_0^{t_{aq}} Nu_z(t)dt \tag{4}$$

Generally speaking, the relative error on the flux measurement thanks to both methods is below 20% for each measurement point.

5.2. Results

These two methods have been applied in the present study, and have led to the same profile of the mean local Nusselt number as a function of the local Rayleigh number, measured both in hot and cold boundary layers of the upper three quarters of the cavity. In addition, the second method gives access to the fluctuations of Nu and are plotted **Figure 9**. They are found to be quite significant, reaching up to 100% of the mean value measured at some elevations. A first part where the Nusselt number decreases (Z in [0 ; 0.2]) with small fluctuations. That corresponds to a laminar regime. Then the local Nusselt number increases (Z in [0.2 ; 0.3]) probably due to transition state where we notice a progressive growth of the fluctuations. Finally, This value decreases again (Z in [0.3 ; 1]) with a maximum of fluctuations and extreme values of the Nusselt number, what can be explain by the turbulent state if the flow.

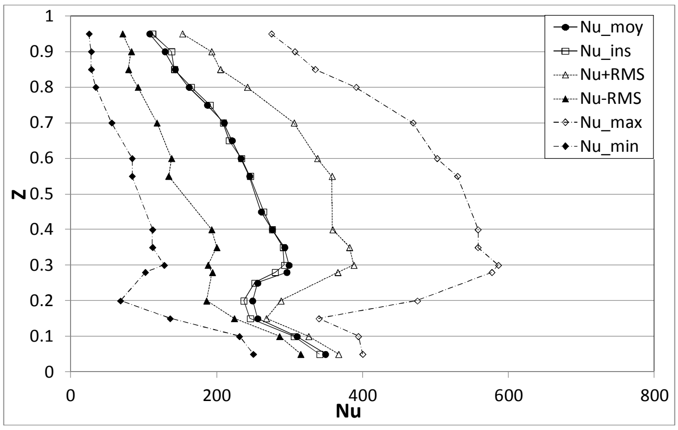

Figure 9. Distribution of the mean, RMS and maximum values of the local Nusselt number along the vertical wall for a Rayleigh number of 1.2×10^{11}.

We can pick out four main trends when plotting Nu_z as a function of the local Rayleigh number, Ra_z, **Figure 10**, four areas come up:

- Nu_z first increases following a laminar $Ra_z^{1/4}$ law for Z below 0.2 ($Ra_z \leq 1.0\times10^9$),
- then, a transition region occurs where Nu_z increases of about 58% in the range $0.2<Z<0.33$ ($1.0\times10^9 \leq Ra_z \leq 4.0\times10^9$),
- Nu_z increases following a turbulent $Ra_z^{1/3}$ law for $0.33<Z<0.90$ ($4.0\times10^9 \leq Ra_z \leq 9.0\times10^{10}$),
- Nu_z finally decreases from $Z>0.9$ up to the top of the cavity ($Ra_z \geq 9.0\times10^{10}$).

The most likely hypothesis to explain the first three evolutions is that the flow successively passes through three zones: laminar, transient and turbulent. The fourth zone seems to result from the interaction of the flow with the top of the cavity.

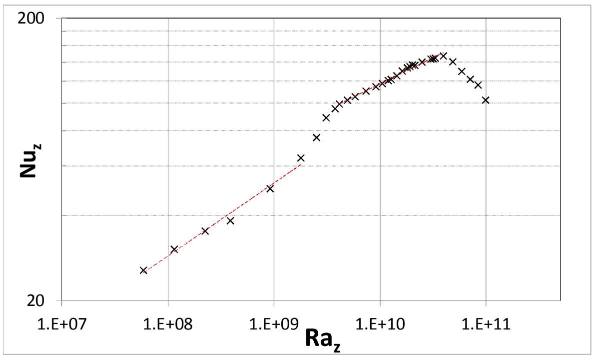

Figure 10. Evolution of the local Nusselt number according to the local Rayleigh number (ΔT=20°C).

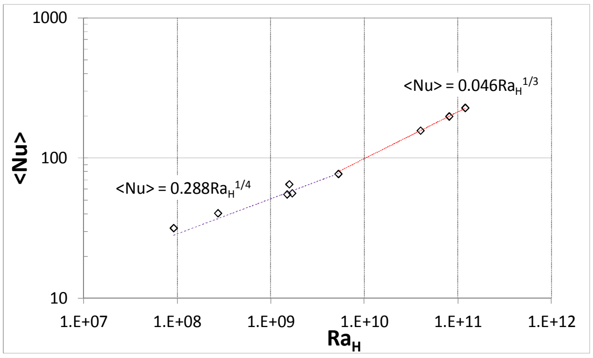

Figure 11. Evolution of the mean Nusselt number as a function of the global Rayleigh number.

Finally, two others Ra_H numbers were considered in this study ($Ra_H=4.0\times10^{10}$ that is to say ΔT=7°C and $Ra_H=8.1\times10^{10}$ for ΔT=14°C) and the global Nusselt numbers were derived. Thanks to these three values and to the results from other previous works [5-7] and [9], we can provide the evolution of the mean Nusselt number, <Nu>, as a function of the global Rayleigh number, Ra_H, **Figure 11**. A change of slope is observed between 1.5×10^9 and 5×10^9, indicating a change in the general flow regime in the cavity, from laminar to turbulent type. We also can notice that the experimental data match relatively accurately with the following correlations:

For $Ra_H \leq 1.0\times10^9$, $\langle Nu\rangle = 0.288\times Ra_H^{1/4}$ (5)

For $1.0\times10^9 < Ra_H \leq 1.2\times10^{11}$ $\langle Nu\rangle = 0.046\times Ra_H^{1/3}$ (6)

Correlation for the laminar regime (eq.(5)) fits very well the numerical values obtained for example by Henkes [10] (i.e. $\overline{Nu}Ra_H^{-1/4}$=0,30).

6. Conclusion

The first observation of this paper is the perfect centrosymmetry of the flow within the cavity. It allows to conduct the studies over only one half of the cavity. Then, we noticed that the thermal boundary layer thickness along the temperature controlled walls thickness is affected by recirculation zones in the upper part of the cavity. Moreover, when observing temperature fluctuations, kurtosis and skewness, a specific position comes out in the thermal boundary layer where the fluctuations reach a maximum.

Finally, a Nusselt correlation as a function of the local Rayleigh number has been derived for Z>0.3 and a 20°C temperature difference between the two walls. Results from the present studies, added to those coming from previous works at lower Ra [5-7] provide a complete correlation for the Nusselt number over a wide range of Rayleigh numbers, from laminar to turbulent developed regimes.

Acknowledgements

The authors gratefully acknowledge the financial support provided by the interdisciplinary program “Energy” from CNRS. They also thank Mr. Hervé Arlaud for its contribution.

References

[1] De Vahl Davis G 1968 Laminar natural convection in an enclosed rectangular cavity *Int. J. of Heat and Mass Tr.* **11** 1675–93

[2] Trias F X, Soria M, Oliva A and Pérez-Segarra C D 2007 Direct numerical simulations of two- and three-dimensional turbulent natural convection flows in a differentially heated cavity of aspect ratio 4 *J. of Fluid Mech.* **586** 259–93

[3] Le Quéré P and Penot F 1989 Numerical and experimental investigation of the transition to unsteady natural convection of air in a vertical differentially heated cavity
Bau H H and Korpela S A (Eds.) Bifurcation phenomena in thermal processes and convection *ASME HTD* **94** 75–82

[4] Chassaing P 2000 *Turbulence en Mécanique des Fluides* (Toulouse: Cépaduès)

[5] Mergui S 1993 *Experimental Natural and Mixed Convection in an Enclosed Cavity* (Poitiers: Poitiers University)

[6] Salat J 2004 *Contribution to the Study of Three-Dimensional Natural Convection in Differentially Heated Cavity* (Poitiers: Poitiers University)

[7] Skurtys O 2004 *A Contribution to Flow Control of Natural Convection by Thermal Excitation of the Boundary Layers in Differentially Heated Cavity* (Poitiers: Poitiers University)

[8] Saury D, Rouger N, Djanna F and Penot F 2011 Natural convection in an air-filled cavity: experimental results at large Rayleigh numbers *Int. Com. in Heat and Mass Tr.* **38** 679–87

[9] Tian Y S and Karayiannis T G 2000 Low turbulence natural convection in an air filled square cavity Part I: the thermal and fluid flow fields *Int. J. of Heat and Mass Tr.* **43** 849–66

[10] Henkes R A W M 1990 *Natural Convection Boundary Layers* (Delft: Delft University of Technology)